Scanning Electron Microscopy

Volume 1985
Number 2 *Part II*

Article 12

5-17-1985

Analysis of Backscattered Electron Signals for X-Ray Mask Inspection

Michael G. Rosenfield
IBM T.J. Watson Research Center

Follow this and additional works at: https://digitalcommons.usu.edu/electron

Part of the Biology Commons

Recommended Citation

Rosenfield, Michael G. (1985) "Analysis of Backscattered Electron Signals for X-Ray Mask Inspection," *Scanning Electron Microscopy*: Vol. 1985 : No. 2 , Article 12.
Available at: https://digitalcommons.usu.edu/electron/vol1985/iss2/12

This Article is brought to you for free and open access by the Western Dairy Center at DigitalCommons@USU. It has been accepted for inclusion in Scanning Electron Microscopy by an authorized administrator of DigitalCommons@USU. For more information, please contact digitalcommons@usu.edu.

SCANNING ELECTRON MICROSCOPY/1985/II (Pages 605-615)
SEM Inc., AMF O'Hare (Chicago), IL 60666 USA

0586-5581/85$1.00+.05

ANALYSIS OF BACKSCATTERED ELECTRON SIGNALS FOR X-RAY MASK INSPECTION

Michael G. Rosenfield

IBM T.J. Watson Research Center
P.O. Box 218
Yorktown Heights, NY 10598
Phone No.: 914-945-2727

(Paper received January 31 1985, Completed manuscript received May 17 1985)

Abstract

A rapid and automated inspection system is a necessity for the detection of defects in x-ray and optical lithography masks. The design of an electron-beam mask inspection system requires a complete understanding of the backscattered electron signal from the various defects which will be encountered. A Monte Carlo simulation program has been used to study the effects of electron-beam size, detector placement, defect type, electron-beam voltage, and absorber thickness on the back-scattered electron signal.

Keywords: Backscattered electron signals, Monte Carlo, X-Ray mask inspection, electron-beam lithography, scattering, simulation, beam size, defects, material thickness requirements, detector placement.

Introduction

A rapid and automated inspection system is a necessity for the detection of defects in x-ray and optical lithography masks. As masks become more complex and critical feature sizes shrink below one micron, the limits of optical inspection systems become apparent. Presently, it is impossible to reliably detect submicron defects in submicron mask patterns with commercial inspection systems. However, the use of an electron-beam lithography system, with its high resolution and overlay capabilities will make it possible to inspect submicron mask patterns for defects. Mask inspection is a natural extension of an electron-beam system since the data used to write the mask can be used to inspect it as well. Electron-beam techniques have been suggested and/or applied to mask inspection by several groups.[7,8,18,27,28,31] In this paper we will attempt to characterize the different influences on the backscattered electron signals from structures encountered during mask inspection.[24]

Conceptually, the idea of using an electron-beam system to perform the mask inspection function is simple. Mask defects can be detected by a comparison of a signal from the mask with the design data used by the electron-beam system to write the mask[28] (and R.A. Simpson, private communication). Thus, the presence or absence of masking material must be detected in some way. Low energy (< 50eV) secondary electrons, generated near the surface by the inelastic scattering of primary and backscattered electrons with loosely bound outer electrons, are often used to form images in scanning electron microscopes (SEMs).[5,23,32] Secondary electrons yield topographical information since they are generated near the surface of the structure. High energy backscattered electrons have also been used in SEMs[21,22,33] and are widely accepted for use in electron-beam lithography systems for detection of registration marks.[2,16,30] Backscattered electrons are produced by the elastic scattering of the incident electrons with the nuclei of the target material or with the electron clouds surrounding the nuclei. The energy of backscattered electrons can range almost up to the incident beam energy and also yield information about the material make-up of the target structure.

Backscattered electrons are desirable for registration in electron-beam systems since they allow for the detection of registration marks through resist or other process related planarizing coatings.[2,16,30] Backscattered electrons are also favored in lithography systems for a very practical reason – backscattered

electron detectors are simple to install inside the electron-beam chamber and do not require large bias voltages. These voltages create electric fields which can negatively influence the electron-beam as it is writing a pattern. As far as x-ray mask inspection is concerned, backscattered electrons are also favored because of the larger signal difference between high and low atomic number materials as compared to secondary electrons.[6] For these reasons we will investigate backscattered electron signals in this paper.

An in-depth understanding of the backscattered electron signal is therefore necessary in order to achieve the best possible signal for comparison to design data. A new Monte Carlo simulation program[7,15,19–20] was written to study the effects of electron-beam size, backscattered electron collection range (or detector placement), defect type, electron-beam voltage, and absorber thickness on the signal from different structures. Good agreement with experimental backscattered electron signals gave confidence in using the Monte Carlo program for these investigations.[24,26]

After a brief review of the Monte Carlo program used in these studies, we will show the effects of different detector placement on the backscattered electron image. The effects of incident electron-beam size and different take-off angle ranges on the signal will then be discussed in a quantitative manner. The required gold thickness for the maximum signal will be determined for various beam energies. Required chrome thickness will also be determined and we will see that the required thickness can be related, in a universal fashion, to the Gruen and Bethe ranges of the electrons in the scattering material. It will be observed that the backscattered electron signal will drop off if the beam is scanned near the edge of the gold. A universal curve using the Gruen range will be presented to determine at what point inside a gold structure, the electron-beam will see essentially bulk gold. Effects of collection angle range will also be considered.

The Monte Carlo Simulation Program

The Monte Carlo method, in which the trajectories of many incident electrons are followed through a target,[1,4,9–11,13–17,19,20,29] was chosen for the simulation technique. The main reasons for this choice were that the Monte Carlo method is fairly well documented and that it could be modified to investigate the backscattered electron signal from the complicated structures encountered during x-ray mask inspection.

This Monte Carlo computer program has been developed to simulate the backscattered electron signal from a variety of two-dimensional gold on silicon structures expected to be encountered during x-ray mask inspection. The program uses the standard continuous slowing down approximation with the screened Rutherford collision cross-section and Bethe energy loss equation.[14,16] The program, written in Fortran 77, uses some of the techniques introduced by Lin[16,17] to keep track of the electron as it scatters into different areas of the target structure. Whereas Lin's program calculated the backscattered electron signal from an infinitely long resist covered silicon step, this new program is used to simulate the backscattered electron signal from three independent, infinitely long, variable width, variable edge slope, gold lines on a silicon substrate. Through appropriate placement of the three gold on silicon lines, the backscattered electron signal from different types of defects typically found on x-ray masks or mask copies can be simulated. Although gold on silicon was primarily simulated, other combinations such as PMMA on gold or chrome on silicon can be specified. A more detailed description of the operation of the program as well as input and output examples can be found in reference 24.

As is well-known, the Monte Carlo technique involves tracking many electrons incident from a zero width δ-function electron-beam as they scatter through the target. An example which illustrates the program's capabilities is shown in Figure 1, a plot of 15 electron trajectories projected onto the x-z plane. The target is composed of two 0.25 μm full width at half-maximum (fwhm) gold steps and a 0.85 μm fwhm gold step separated by 0.3 μm. The four backscattered electrons in this example can clearly be seen. The energy, take-off angle, azimuthal angle, and position of each backscattered electron is stored and the resulting total energy and number distribution of backscattered electrons are output for the take-off angle, azimuthal angle, and backscatter energy.[24]

A backscattered electron signal for a given structure is calculated by first simulating the δ-function signal. This is done by stepping the position of the incident beam in small (0.0125–0.05 μm) steps over the structure. This process is illustrated in Figure 2. Figure 2 shows the δ-function electron-beam stepped over the target and also the convolution of the δ-function beam with the Gaussian beam shape. This simulates the actual finite sized electron-beam scanning over a target. Note how symmetry of the structure necessitates only one half of the signal being calculated. The distance between δ-function beams is typically much less than the incident beam size. The advantage of this approach is that the δ-function response can be convolved with a variety of beam sizes and shapes. For the simulations to be described here, a Gaussian beam shape was assumed. To save computer time, symmetry was used whenever possible. For the simulations in this paper, 5,000–10,000 electrons per incident δ-function electron-beam were used. The calculations were mostly performed on an IBM 3081 computer. The required CPU time is approximately 1 minute per 1000 trajectories for a 25 kV incident beam voltage.

It has been shown that the simulated energy signal, rather than the number signal, properly takes the backscattered electron energies into account and gives better agreement with experimental signals.[24] This is because the detector used in the experiments and the type most often used in electron-beam lithography systems are diodes whose initial amplification is proportional to the electron's energy. Thus, the energy signal, calculated by adding up the electron energy which is scattered into the specified collection range of the detector, will be used in this paper.

While being useful for comparisons of simulation and experiment, contrast is not a good measure of the quality of the backscattered electron signal. This is because contrast does not contain any information about the signal to noise ratio, SNR, of the signal. It is well known that for high speed inspection of masks with an electron-beam, a high SNR ratio is desirable to guard against false defect detection and the missing of defects[28,31] (and R.A. Simpson, private communication). Assuming a shot noise limited signal, the most noise will be found in the maximum part of the signal and this noise is proportional to the square root of the maximum signal.[16] A parameter, ΔSNR which gives information about the SNR quality of the signal for alignment has been introduced by Lin.[16] For defect

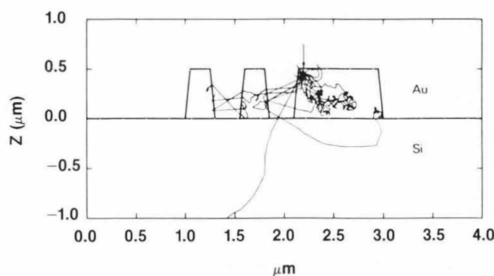

Fig. 1. An example of the Monte Carlo program's capabilities, showing Monte Carlo simulation of electron trajectories. Au thickness = 0.50 μm, beam energy 25 kV, 15 incident electron at X = 2.20 μm.

detection, it is more appropriate to normalize to the energy ΔSNR between 0.5 μm thick gold on silicon and bulk silicon. The ΔSNR can be written:

$$\Delta SNR = \frac{\dfrac{S_{max} - S_{min}}{\sqrt{S_{max}}}}{\dfrac{S_{max-Au} - S_{max-Si}}{\sqrt{S_{max-Au}}}} \quad (1)$$

Note that this parameter is in terms of the energy signal levels and that the normalizing signals from the gold and silicon are total signals covering the entire 90 degrees take-off angle range.

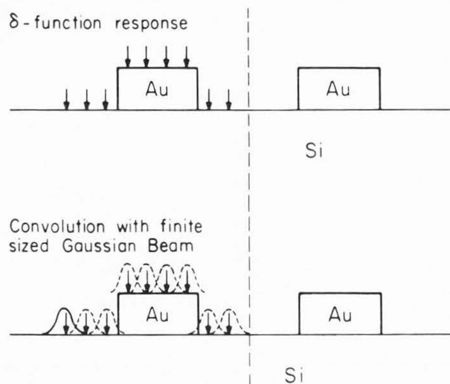

Fig. 2. The process of simulating a backscattered electron signal. First calculate the δ-function response. Then convolve with the desired beam shape. Typically, the beam size will be much larger than the spacing between δ-function electron-beams.

Optimization of Experimental Detector Placement

The optimum placement of the annular diode detector used in the experiments of references 24 and 26 will now be considered. The Monte Carlo program was used to determine the optimum placement of this detector to achieve the best signal from a wide range of structures. The backscattered electron signals from most defects will range from the signal from a small gold step to the signal from a small hole in a gold film. Thus, it is instructive to examine the take-off angle distribution from these two types of defects in order to optimize the placement of the detector.

The simulated energy signals for a 0.25 μm gold step and 0.25 μm hole in a gold film at 25 kV and 0.5 μm gold thickness are shown in Figure 3. A minimum detectable defect size of 0.25 μm and beam fwhm of 0.20 μm was assumed when optimizing the placement of the detector. Vertical sidewalls were used in all simulations. Three different take-off angle ranges corresponding to different detector heights above the wafer surface are shown to illustrate the change in signal as the collection range changes. It can be seen from Figure 3 that the 15–35 degrees range gives the maximum ΔSNR of the three ranges for the gold step. This is expected due to the many electrons which scatter out of the sides of this structure at low angles. However, since the angle distribution from a small hole in a gold film is almost a cosine distribution, it is clear why the 15–35 degrees signal for the 0.25 μm hole has such a poor ΔSNR.

A trade-off is needed so that the signals from the small step and small hole will be maximized. The 30–57.5 degrees take-off angle range, corresponding to a detector height of 6.1 mm above the wafer, is a good compromise as can be seen from Figure 3. A more detailed analysis of ΔSNR's for 25–50, 30–57.5, and 35–62.5 degrees ranges for these structures as well as other various structures[24,26] showed that the 30–57.5 degrees range gives better signal than the other ranges. This qualitative information shows that different defects will scatter electrons into

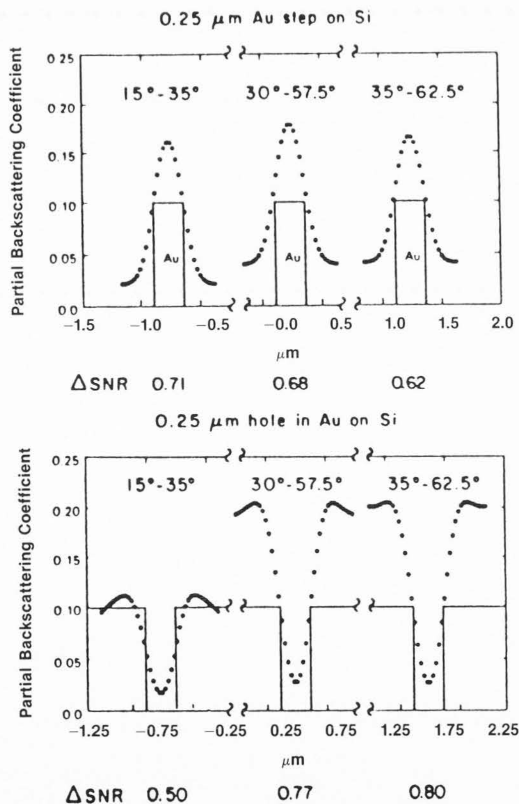

Fig. 3. The simulated energy signals for a 0.25 μm gold step a and a 0.25 μm hole b in a gold film for three different take-off angle ranges. Beam fwhm = 0.2 μm, Au thickness = 0.5 μm, beam energy = 25 kV.

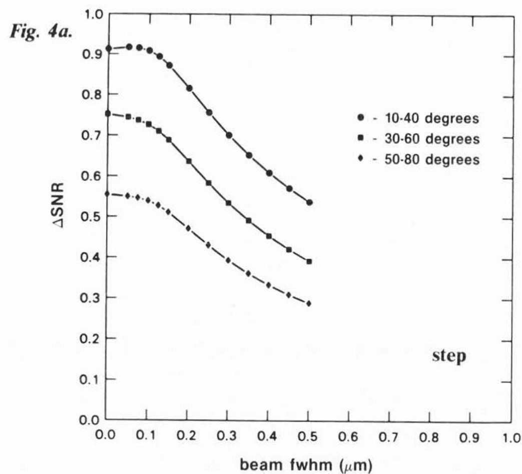

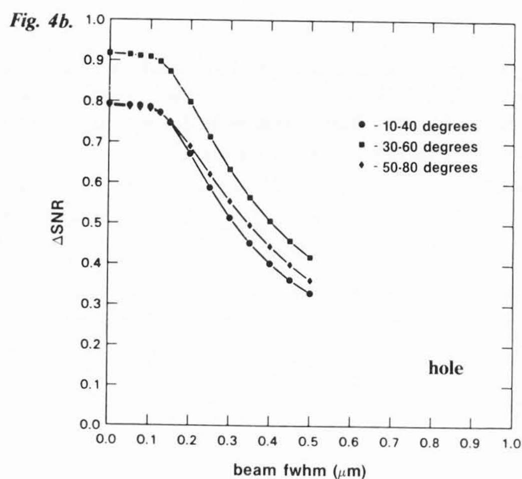

Fig. 4. A plot of ΔSNR versus beam fwhm for the 0.25 μm (a) step and (b) hole at 25 kV beam voltage.

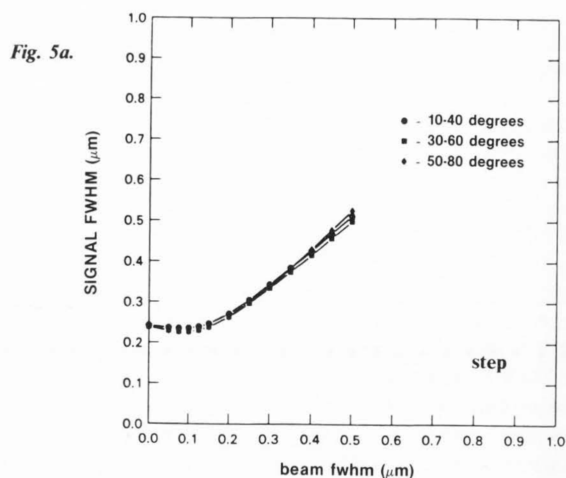

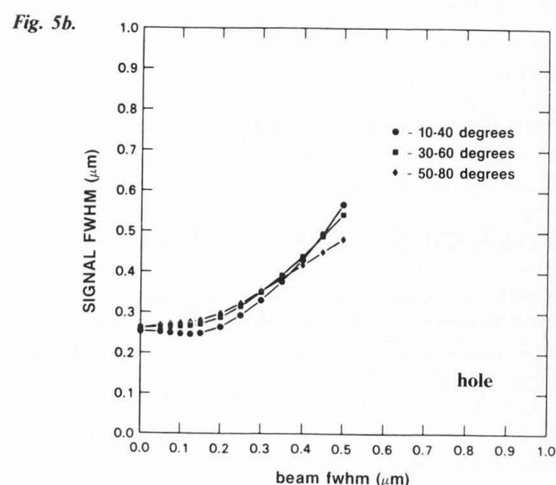

Fig. 5. A plot of signal fwhm versus beam fwhm for the 0.25 μm (a) step and (b) hole at 25 kV beam voltage.

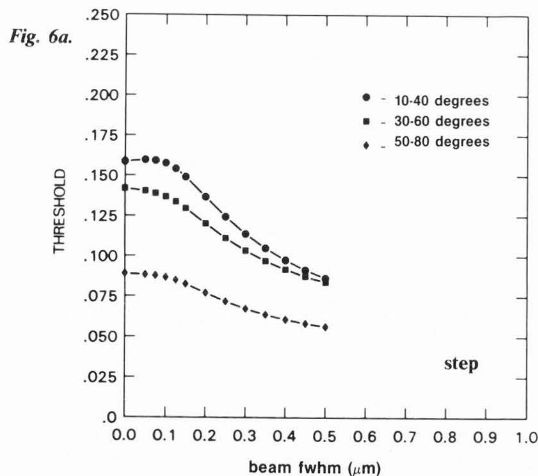

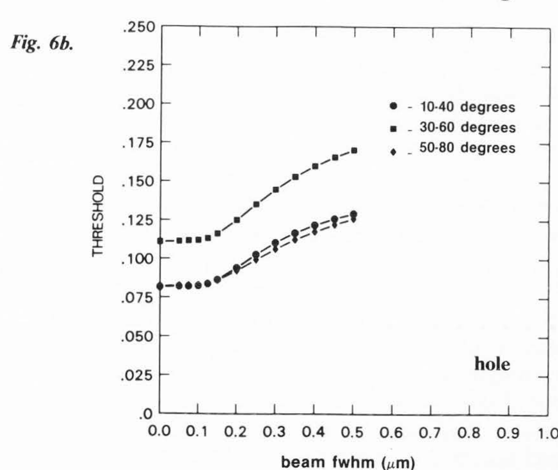

Fig. 6. A plot of threshold versus beam fwhm for the 0.25 μm (a) step and (b) hole at 25 kV beam voltage.

different angle ranges. Thus, unless multiple detectors are used in an inspection system, a tradeoff will be needed to get the best possible signal from all types of defects.

A Study of the Effects of Beam Size and Angle Collection Range

As was shown in the previous section, we can gain much information about the scattering properties of various defects by examining the limiting cases of an isolated gold on silicon step

and an isolated hole in gold on silicon. We are interested primarily in submicron structures since it is the minimum detectable defect size which will influence the design of the mask inspection system.[24,28,29] From a practical viewpoint, an electron-beam system with a 0.25 μm fwhm beam will have much more difficulty detecting a 0.125 μm defect than in detecting a 1.0 or 2.0 μm defect. In this section, the effects of Gaussian beam size (fwhm) and angle collection range on the backscattered electron signal from a 0.25 μm fwhm gold on silicon step with vertical sidewalls and a 0.25 μm hole in gold on silicon with vertical sidewalls will be discussed. The gold thickness is 0.50 μm and the beam energy is 25 kV. Similar studies for other sized structures can be found in reference 24. The effects of beam voltage on the required absorber thickness will be discussed later. The angle ranges of 10–40, 30–60, and 50–80 degrees will be studied. The 0–10 and 80–90 degrees angle ranges were neglected since electrons scattered into these ranges would be extremely difficult to detect inside an electron-beam chamber. All backscattered electron signals were calculated as the energy signal which was shown to give good agreement with experiment.

The effects of beam size and angle collection range will be studied by looking at the backscattered electron signal ΔSNR, fwhm, and threshold. The threshold is defined as the midpoint between the changing signal of interest for a given structure and the bulk signal level of the material surrounding the structure. For example, the threshold for a hole in a gold film would be the midpoint between the level for the bulk gold surrounding the defect and the minimum signal level caused by the hole. Conversely, the threshold for a step or line is the midpoint between the signal for bulk silicon and the high signal generated by the gold step.

ΔSNR

The effects of beam size and angle collection range on the noise quality of the backscattered electron signal from 0.25 μm step and hole structures are shown in Figures 4a and 4b, ΔSNR versus beam size for the different structures simulated. The first observation which can be made is that for submicron step structures, the lower angle range gives the best signal. This is because many electrons exit from the sides of the step at low take-off angles. However, the 30–60 degrees range appears to be best for the holes. This is what was shown in the previous section and implies that if a single detector is used for mask inspection, some type of tradeoff in placement will be required. Note that the 10–40 and 50–80 degrees ranges are almost identical for the hole structures. This agrees with the observation made earlier that holes look like bulk gold except in the immediate vicinity of the defect. Thus, the optimum detector placement for clear defects will be the same as for bulk gold. The fundamental shot noise limitations of the backscattered electron signals are discussed in references 24 and 25.

As far as the effects of beam size are concerned, a degradation in ΔSNR starts when the beam size becomes at least four-tenths of the structure fwhm. For the steps, a 25 percent loss of ΔSNR occurs when the (beam fwhm)/(structure fwhm) ratio is about 1.2. Similar results are seen for the holes with a 25 percent reduction in ΔSNR being observed at a ratio of about 1.1.

Backscattered Electron Signal Fwhm

The effects of beam size and angle collection range on the fwhm of the backscattered electron signals from the 0.25 μm structures are shown in Figures 5a and 5b. As would be expected, the lower angle range tends to give a signal fwhm which is closer to the actual fwhm of the structure. This becomes more apparent as the structure size increases.[24] For the smaller structures, 0.25 μm and below, the angle collection range does not appear to have a significant influence on the signal fwhm. For the larger structures, in which the two sides of the structure are isolated (as far as the electrons are concerned), the higher angle range gives a smaller signal fwhm than the lower ranges. This is because the electrons scattering near the edge are concentrated in the lower angle ranges; therefore, the signal rises more slowly if only higher angles are collected. Generally, and especially for the middle angle ranges, the signal fwhm from steps are slightly smaller than the step fwhm and signals from holes are slightly larger than the hole fwhm. This, of course, pertains to beam sizes which do not significantly affect the signal fwhm. The discrepancy of signal fwhm and structure fwhm has implications when using an electron-beam system or SEM for line-width measurement.[12,18]

Generally, the signal fwhm is fairly constant for small beam sizes and then begins to increase steadily when the incident beam size becomes larger than about 0.4–0.5 of the structure fwhm. In other words, there are two distinct regions of the signal fwhm versus beam fwhm curves. The first is the level area of the curve in which material and scattering properties dominate and the other is the rising area of the curve in which the beam size dominates. For steps, a signal fwhm 50 percent larger than the structure fwhm occurs for a (beam fwhm)/(structure fwhm) ratio of about 1.3–1.4. For holes, a 50 percent increase is seen for a ratio of about 1.1–1.2. This has implications in mask inspection if the desired minimum detectable defect size is smaller than the probing electron-beam. Depending on the threshold setting of the comparator used to digitize the signal, the detected size of the defect could be considerably larger than the actual size.

Threshold (DC Level)

The threshold, or midpoint between high and low signal levels, will change with increasing beam size. For small steps, the high signal level will drop towards the silicon level as the beam size becomes larger than the structure. In other words, the presence of the structure has less of an effect on the scanning beam. A similar process occurs for holes in a gold film with the minimum signal level rising towards the gold signal level as the beam size increases. Graphs of threshold versus beam fwhm are shown in Figures 6a and 6b for 0.25 μm structures. The units for the threshold are in terms of the partial energy signal.

As would be expected for holes, the 10–40 and 50–80 degrees angle collection ranges have essentially the same thresholds. The 30–60 degrees range gives higher thresholds since the high signal level is larger. For the 0.25 μm and smaller step structures, the lower angle ranges give higher thresholds. As the structure size increases, the 30–60 degrees range gives a higher threshold since the maximum signal level is generated from an area which, to the electrons, almost resembles bulk gold.[24]

It can be seen by examining Figure 6 that for a given beam size,

there is a difference in threshold or DC level between steps and holes. The threshold of a signal is a complex function of the beam size, beam voltage, structure size, and detector configuration. The DC level difference is important since in most cases a comparator threshold wil have to be set so that the mask inspection system can electronically determine the presence or absence of masking material. As has been discussed in refs. 24, 25, 28 and by R.A. Simpson (private communication), the placement of the comparator threshold, in relation to the high and low signal levels, will greatly influence the SNR characteristics of the backscattered electron signal. The importance of correct threshold settings can be seen in Figure 7 which shows the backscattered electron signals for a 0.50 μm fwhm beam scanning over 0.25 μm defects.

Absorber Thickness Studies

The previous section was concerned with the effects of beam size and angle collection range on structures with a fixed 0.50 μm gold thickness and with a fixed incident 25 kV electron-beam energy. To repeat the work of the previous section for every combination of defect type, gold thickness, and beam energy would clearly be impossible. Therefore, we will look at infinite films on silicon to gain an understanding of the film thickness requirements for maximum signal levels in mask inspection. Gold on silicon as well as chrome on silicon films will be considered. The simulations were done by calculating the energy backscatter coefficients for a single δ-function electron-beam incident on different thicknesses of gold and chrome on silicon.

One of the goals of this study was to see if some simple rules of thumb could be developed for absorber thickness requirements. In his study on alignment signals, Lin,[16] introduced a quantity, Z, which was the step depth of the silicon alignment mark normalized to the Bethe range of the electrons in silicon. By normalizing to the Bethe range, Lin obtained universal curves describing the alignment signal characteristics for beam energies ranging from 5–30 kV.[16]

A similar technique was used in this study by plotting the backscatter coefficient versus film thickness normalized to the Gruen range.[3]

$$R_G = 0.04 \frac{E_o^{1.75}}{\rho} \quad (2)$$

where E_O is the incident beam energy in kV, ρ is the density in g/cm^3, and R_G is in μm. Note that many authors use 0.046 instead of 0.04 in their expression for the Gruen range. The expression containing 0.046 was Gruen's original expression for electron energy dissipation in air.[3] In any case, it is only a constant and will not have an effect on the results obtained in this study. Values for R_G and R_B, the Bethe range, for gold, chrome, and silicon at different beam energies are listed in Figure 8. It is important to remember that R_B is calculated using the Monte Carlo program while the Gruen range expression originally was derived from experimental observations.

Figure 9a is a plot of the total energy backscatter coefficient η_E, versus gold thickness normalized to the Gruen range of electrons in gold, normalized to the Gruen range. Figure 9b is similar except that the gold thickness is normalized to the Bethe range. Figures 10a and 10b are similar except that the total number backscatter coefficient, η_B is used. A range of beam voltages from 10 to 30 kV is shown and it can be seen that a universal relationship is obtained by normalizing the gold thickness to R_B or R_G. It can be seen from these curves that η_B reaches 90 percent of its maximum at a gold thickness of approximately 0.15 R_B or 0.37 R_G. The more important, from a simulation and practical viewpoint, η_E reaches 90 percent of its peak about 0.13 R_B or 0.33 R_G. The thickness requirements for η_E are slightly lower than those for η_B since η_B weights all electrons the same, even though those backscatter electrons scattered from deep in the gold will have a very low energy. These electrons will not contribute a significant amount to the signal since most backscattered electron detectors are energy sensitive. Universal curves from partial angle ranges (10–40 and 30–60 degrees) were found to give similar results as those shown in Figures 9 and 10. This is expected since there is no surface topography to influence the electron scattering. Experimental results at 25 kV also agreed well with Figure 9a (R.A. Simpson, private communication).

As was previously mentioned, R_B must be calculated using the Monte Carlo program or else by interpolation on a universal curve.[3] The Gruen range can be calculated by anyone possessing a periodic table. It is because of this ease of calculation that R_G will be used when normalization is required for all of the following discussion. The universal quality of the curves of Figures 9 and 10 is very interesting since the values for η_B and η_E were calculated using the Monte Carlo program while the normalization factor was calculated using an unrelated empirically derived equation.

Universal curves for chrome films on silicon are shown in Figure 11. Note that the difference between maximum and minimum signal levels is much less for chrome as compared to gold, which has a higher atomic number. There is more scatter in the curves; but, the results are essentially the same as for gold. The increased scatter may be due to different materials having slightly different exponents in the R_G expression at different beam voltages.[3] However, a good rule of thumb is that to obtain more than 90 percent of the available signal, a film thickness greater than 0.33 R_G is required. For a 25 kV electron-beam, a gold thickness of about 0.2 μm would be required.

Effects of Scanning Near the Edges of a Structure

We have seen the increased scattering into lower take-off angles for submicron step structures and have observed the effects of different angle collection ranges. A practical problem, as far as inspection is concerned, caused by these scattering effects is that the backscattered electron signal does not instantly rise to a maximum signal as soon as the beam begins scanning over a step or into a hole. This is a function of electron scattering and the incident beam size and is true even for very small fwhm electron-beams or the δ-function beam. The electron-beam must be somewhat inside the structure before the signal reaches a maximum (or minimum). How far inside the structure will depend on the angle collection range, the beam size, and the beam voltage. This effect is most important if one is adopting a mask inspection scheme[27,28] in which the inside or positive areas of a mask are scanned for clear defects and the outside or negative areas are scanned for opaque defects. A dead zone or non-inspection area is left around all shapes to allow for registration error. The problem is that if the dead zone region is small,

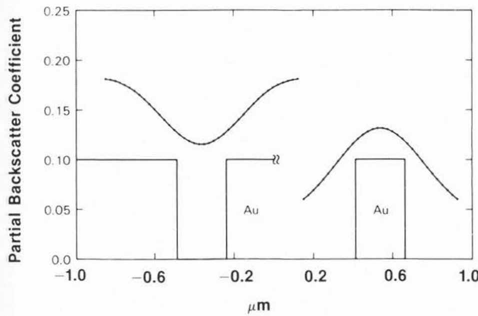

Fig. 7. Partial energy backscatter signals (20.0–50.0 degrees) for 0.25 μm defects scanned by a 0.5 μm fwhm beam. Partial energy signal = 20.0–50.0 degrees, 0.25 μm Au on Si structures, beam fwhm = 0.50 μm, Au thickness = 0.50 μm, beam energy = 25 kV.

Gruen and Bethe Ranges

Beam Voltage	Au		Cr		Si	
kV	R_G (μm)	R_B (μm)	R_G (μm)	R_B (μm)	R_G (μm)	R_B (μm)
10	0.12	0.40	0.31	0.60	0.97	1.44
20	0.39	1.19	1.05	1.97	3.24	4.84
25	0.58	1.50	1.56	2.91	4.80	7.50
30	0.80	2.32	2.14	4.01	6.60	9.97

Fig. 8. Gruen and Bethe ranges for gold, chrome, and silicon at different beam voltages.

Fig. 9a.

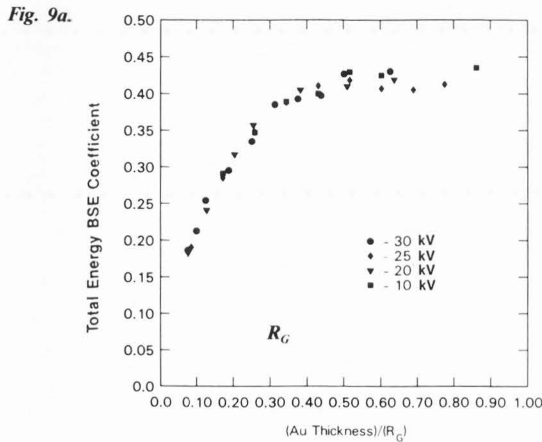

Fig. 10a.

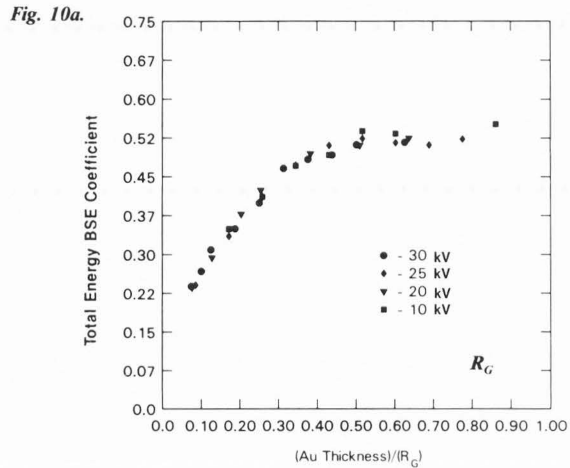

Fig. 9b.

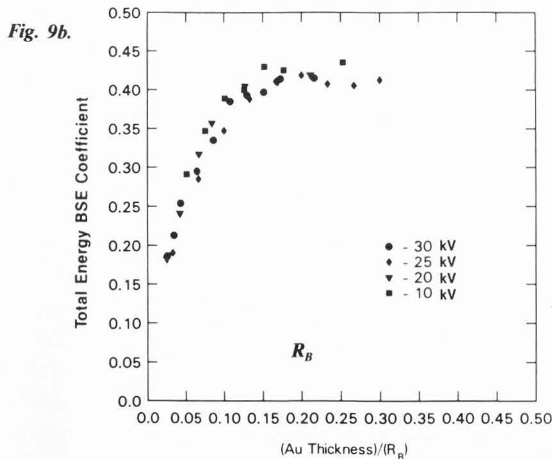

Fig. 10b.

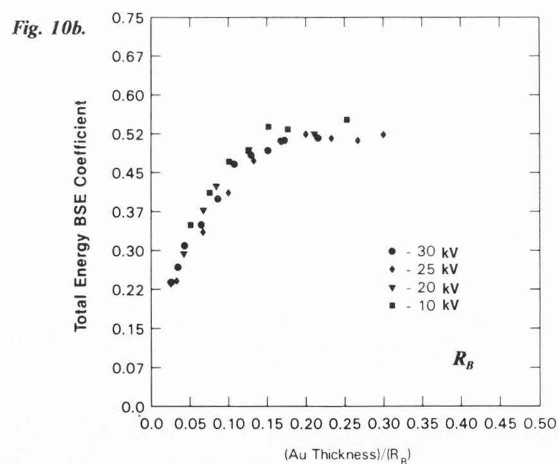

Fig. 9. A universal plot of η_E versus gold thickness normalized to (a) R_G and (b) R_B for different beam voltages. The substrate material is silicon.

Fig. 10. A universal plot of η_B versus gold thickness norma. ized to (a) R_G and (b) R_B for different beam voltages. The substrate material is silicon.

Fig. 11a.

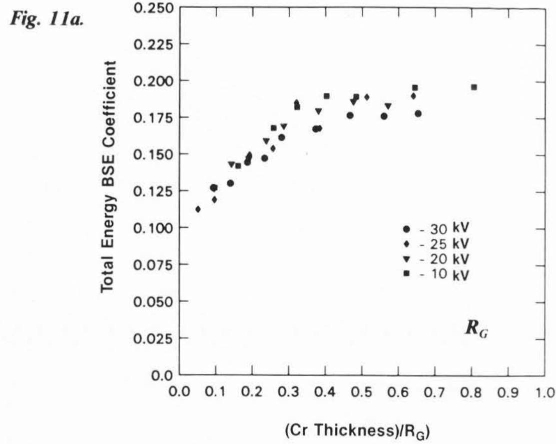

Fig. 11b.

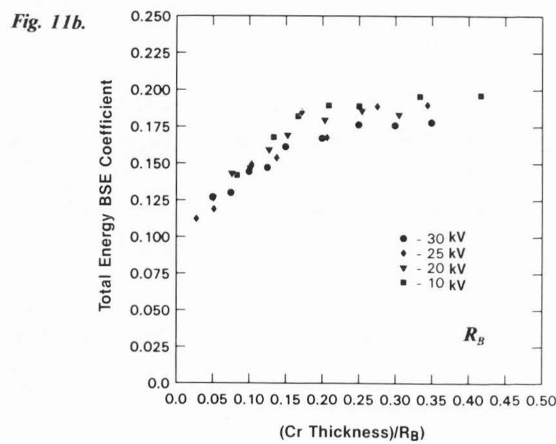

Fig. 11. A universal plot of η_E versus chrome thickness normalized to (a) R_G and (b) R_B for different beam voltages. The substrate material is silicon.

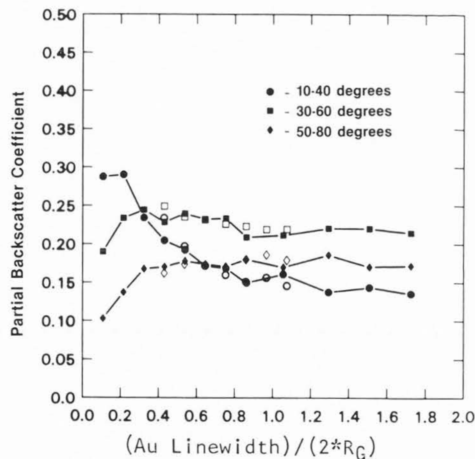

Fig. 13. A plot of η_E versus normalized gold linewidth to illustrate the effect of scanning near a structure's edge. The δ-function beam is incident at the center of a gold step on silicon. The gold thickness is 0.5 μm. The dark symbols are for a 25 kV beam voltage and the open symbols are for a 10 kV beam voltage.

Fig. 12a.

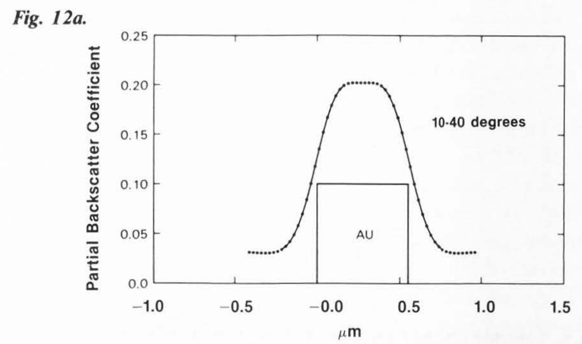

Fig. 12b.

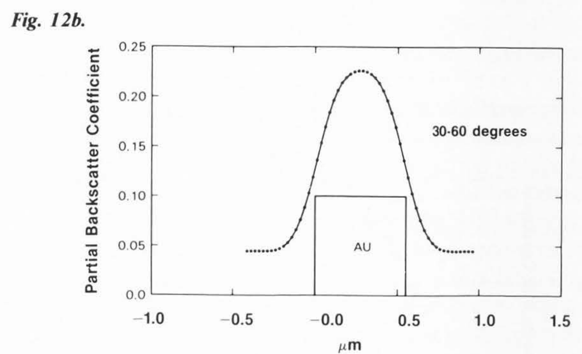

Fig. 12c.

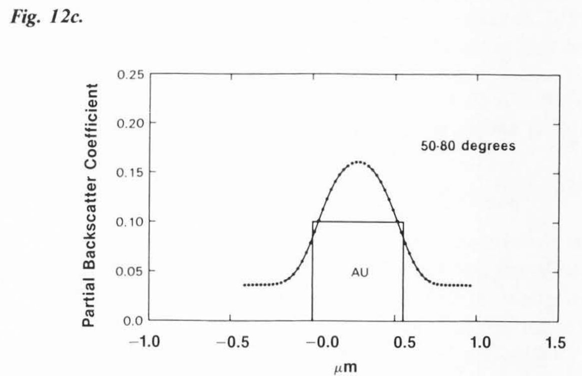

Fig. 12. A simulated backscattered electron signal to show the fall off of the signal near the structure's edge. Partial energy signal (a) 10.0–40.0 degrees, (b) 30.0–60.0 degrees and (c) 50.0–80.0 degrees.

it is possible that the backscattered electron signal level could drop when the beam scans near the edge of a gold structure. A complementary occurrence takes place when the beam is scanning on silicon in the vicinity of a gold structure. In this case, the signal rises because of overlap of the beam onto the gold. These changes in signal levels, depending on the comparator threshold settings, could cause false defects to be detected.

The effect is illustrated in Figures 12a–12c, showing the backscattered electron energy signal for a 0.55 μm gold step on silicon. The beam fwhm is 0.25 μm, the beam energy is 25 kV, and the gold thickness is 0.46 μm. The signal can be seen to drop off 0.1–0.2 μm inside the step for the 30–60 and 50–80 degrees angle ranges. This reduced signal is what would be detected if the electron-beam was scanning near the edges of that shape.

A simulation experiment was conducted to further investigate the effect of the signal level dropping near the edges of gold shapes. The partial energy backscatter coefficient was plotted versus half the step linewidth (or distance from the δ-function beam to the shape edge) normalized to the Gruen range. The results for the three angle ranges and 10 and 25 kV beam energies are shown in Figure 13. A sharp drop in signal occurs for the 50–80 degrees range starting about 0.33 R_G from the edge. For the 30–60 degrees range, the signal begins to drop off about 0.2 R_G from the edge. The signal actually increases if the lower angle range is used. A possible compromise would be to collect backscattered electrons in the 20–50 degrees angle range.[25] In this case, there would only be a 6 percent loss of signal from bulk materials and a significant increase in the signal level near the edges of steps.

Conclusion

The design and implementation of a high resolution mask inspection system using an electron-beam probe is a difficult task. Many different areas must be investigated and understood before a reliable high speed inspection system can be built. In this paper, we have discussed the fundamental characteristics of the backscattered electron signal used to detect the presence or absence of masking material.

A Monte Carlo program has been developed to simulate the backscattered electron signal from the complicated structures encountered in mask inspection. The program is based on the standard continuous slowing down approximation, Bethe energy loss equation, and the screened Rutherford collision cross-section. It was found that the simulated energy signal, the total energy of the electrons striking the detector, gave good agreement with experiment for different submicron structures, collection angle ranges, beam voltages, gold thicknesses, and beam sizes. This excellent agreement with experiment was important since it gave confidence in using the program to investigate the backscattered electron signal properties of interest for mask inspection.

It has been shown that electrons scattered into the middle take-off angle ranges (30–60 degrees from the plane of the target) gave the best overall backscattered electron signal quality for clear and opaque defect structures. Although the 30–60 degrees range is best overall, the signal for submicron step structures can be enhanced by also collecting the lower angle backscattered electrons. Practical constraints, such as the effects of the beam scanning near the edge of a structure, also make it necessary to collect some low angle electrons.

The effect of electron-beam size on the backscattered electron signal characteristics was also described. A Gaussian electron-beam shape was used in the simulation. A quantity, ΔSNR, was used as a figure of merit for the noise quality of the signal. Curves of ΔSNR, signal fwhm, and threshold (DC level) versus beam fwhm were presented for a variety of submicron gold on silicon structures over three different angle ranges. A fall off in ΔSNR was found to begin to occur when the beam size becomes about 0.4 of the structure fwhm. For steps, a 25 percent loss of ΔSNR occurs when the (beam fwhm)/(structure fwhm) ratio is about 1.2. Similar results are seen for holes with a 25 percent reduction in ΔSNR being observed at a ratio of about 1.1.

It was observed that the graph of signal fwhm versus beam fwhm has two distinct regions for various structures. There is a flat region for beam sizes up to about 0.5 of the structure fwhm and a region for larger beam sizes in which the signal fwhm rises steadily with the beam fwhm. For steps, a signal fwhm 50 percent larger than the structure fwhm occurs for a (beam fwhm)/(structure fwhm) ratio of about 1.3–1.4. For holes, a 50 percent increase is seen for a ratio of about 1.1–1.2. It was also found that the thresholds or DC levels of the signals from step and hole structures are different and behave in different manners as the beam size is increased. For steps, the threshold drops towards the silicon signal level as the beam size increases. For holes, the threshold rises toward the gold signal level.

Universal curves for various beam energies showed that to collect 90 percent of the available backscattered electron signal, the scattering material should be about 0.13 R_B or 0.33 R_G thick. It is desirable to use the Gruen range, R_G since it is easily calculated using a simple analytical expression. The universal relationship of the backscatter coefficients to material thickness normalized to R_G is interesting because the backscatter coefficients are calculated using the Monte Carlo program while R_G is calculated using an empirically derived equation. Similar universal curves were introduced to illustrate the effect of scanning the electron-beam near the edges of shapes. As the beam scans near the shape edges, it is possible that the backscattered electron signal can fall off. If low take-off angle electrons are collected, an increase in signal is observed. For a 30–60 degrees angle collection range, the signal begins to drop off at about 0.2 R_G from the edge while for a 50–80 degrees range the signal begins to drop off at about 0.33 R_G from the edge. This decrease in signal level is important since it can cause the signal to fall below the comparator threshold used for determining the presence or absence of masking material. Collecting backscattered electrons in the 20–50 degrees range should reduce the drop in signal near a step edge with only a 6 percent loss in signal from bulk materials.

There are several areas in which further work is needed. It would be interesting to extend the Monte Carlo program to simulate three dimensional structures. Also, a study of more complicated defect structures, besides steps and holes, could be performed with the program in its present form. In this research, we have mainly looked at the backscattered electron signal. It would be worthwhile to extend the simulation so that the secondary electron signal could be simulated as well. The signal and SNR characteristics of the backscattered and secondary electron signals could then be compared for the inspection of low atomic number material combinations, such as resist on silicon.

Mask inspection is one of the few areas remaining in the electron-beam system field which has not been fully explored.

It is hoped that this work will be of use to others interested in the development of high resolution mask and wafer inspection systems.

Acknowledgements

The author would like to thank Andrew R. Neureuther for his guidance, support, and friendship. This work is a collaborative study supported in part by the IBM T.J. Watson Research Center and the National Science Foundation under grant ECS-8106234.

References

1. Adesida I. (1979). Electron energy dissipation in layered media. Ph.D. Dissertation, University of California, Berkeley.

2. Davis DE. (1980). Registration mark detection for electron-beam lithography–ELI system. IBM J. Res. Develop. **24(5)**: 545-553.

3. Everhart TE, Hoff PH. (1971). Determination of kilovolt electron energy dissipation vs. penetration distance in solid materials. J. Appl. Phys. **42(13)**: 5837-5846.

4. George EP, Robinson VNE. (1976). The dependence of SEM contrast upon electron penetration. Scanning Electron Microsc. 1976: I: 17-26.

5. Goldstein JI, Newbury DE, Colby JW, Yakowitz H, Lifshin E, Coleman JR. (1975). Practical Scanning Electron Microscopy, Goldstein JI, Yakowitz H. (Eds.), Plenum Press, New York.

6. Goldstein JI, Newbury DE, Echlin P, Joy DC, Fiori C, Lifshin E. (1981). Scanning Electron Microscopy and X-Ray Microanalysis. Plenum Press, New York. Also, see reference 5.

7. Goto Y, Furukawa Y, Inagaki T. (1978). Inspection for defects of a mask containing one- to submicrometer patterns using a scanning electron microscope and feature extraction method. J. Vac. Sci. Technol. **15(3)**: 953-956.

8. Grobman WD. (1980). Mask inspection using electron-beam systems. IBM Technical Disclosure Bulletin, **22(12)**: 540.

9. Hawryluk RJ, Hawryluk AM, Smith HI. (1974). Energy dissipation in a thin polymer film by electron beam scattering. J. Appl. Phys. **45(6)**: 2551-2566.

10. Heinrich KFJ, Newbury DE, Yakowitz H. (1976). Use of Monte Carlo Calculations in Electron Probe Microanalysis and Scanning Electron Microscopy. National Bureau of Standards, Washington, D.C., Special Publ. 460.

11. Hembree GG, Jensen SW, Marchiando JF. (1981). Monte Carlo simulation of submicrometer linewidth measurements in the scanning electron microscope. In: Microbeam Analysis–1981 (Geiss RH. (Ed.), San Francisco Press, San Francisco, 123-126.

12. Jensen SW, Swyt D. (1980). Sub-micrometer length metrology: problems, techniques, and solutions. Scanning Electron Microsc. 1980; I: 393-406.

13. Kato Y, Takigawa T, Yoshimi M, Kawabuchi K. (1982). Mark detection in high voltage electron beam lithography. (Colloque Intl. Sur la Microlithographie), Sitecmo Dieppe, Paris, France. Proceedings of Microcircuit Engineering, 28-33.

14. Kyser DF. (1981). Monte Carlo calculations for electron microscopy, microanalysis, and microlithography. Scanning Electron Microsc. 1981; I: 47-62.

15. Kyser DF, Murata K. (1974). Monte Carlo simulation of electron beam scattering and energy loss in thin films on thick substrates. Proceedings of the 6th International Conference on Electron and Ion Beam Science and Technology, Bakish R. (Ed.), Electrochemical Society, Princeton, NJ, 205-223.

16. Lin YC. (1981). Alignment Signals From Electrons Scattering Near an Edge for Electron Beam Microfabrication, Ph.D. Dissertation, University of California, Berkeley.

17. Lin YC, Neureuther AR. (1981). Alignment signals from resist-coated marks for direct wafer writing. IEEE Trans. Electron Devices, **ED-28(11)**: 1397-1405.

18. Migitaka M, Mizukami K, Hisamoto Y, Wada Y. (1982). An automated VLSI-mask inspection system. J. Vac. Sci. Technol. **20(1)**: 26-32.

19. Murata K. (1982). Monte Carlo simulation of electron scattering in resist film/substrate targets. Proceedings of the 1st Pfefferkorn Conf., Electron Beam Interactions with Solids. D.E. Kyser, H. Niedrig, D.F. Newbury, R. Shimizu (Eds.), SEM, Inc., AMF O'Hare, IL, 311-330.

20. Murata K, Nomura E, Nagami K, Kato T, Nakata H. (1979). Experimental and theoretical study of cross-sectional profiles of resist patterns in electron-beam lithography. J. Vac. Sci. Tech. **16(6)**: 1734-1738.

21. Robinson VNE. (1980). Imaging with backscattered electrons in a scanning electron microscope. Scanning, **3(1)**: 15-26.

22. Robinson VNE. (1975). Backscattered electron imaging. Scanning Electron Microsc. 1975; 51-60.

23. Robinson VNE, George EP. (1978). Electron scattering in the SEM. Scanning Electron Microsc. 1978; I: 859-868.

24. Rosenfield MG. (1984). Analysis of Backscattered Electron Signals for X-ray Mask Inspection. Ph.D. Dissertation, University of California, Berkeley.

25. Rosenfield MG, Goodman DS, Neureuther AR, Prouty MD. (1985). A comparison of backscattered electron and optical images for submicron defect detection. J. Vac. Sci. Technol. B, **2(1)**: 377-382.

26. Rosenfield MG, Neureuther AR, Viswanathan R. (1983). Simulation of backscattered electron signals for x-ray mask inspection. J. Vac. Sci. Technol. B, **1(4):** 1358-1363.

27. Rosenfield MG, Viswanathan R, Wilson AD, Vettiger P, Neureuther AR. (1982). X-ray mask inspection using a vector scan electron-beam system, Proceedings of Microcircuit Engineering, Op. Cit., 179-182.

28. Simpson RA, Davis DE. (1982). Detecting submicron pattern defects on optical photomasks using an enhanced EL-3 e-beam lithography tool. Proc. Society of Photooptical & Instrumentation Engineers, **334**. (Copy available from SPIE, P.O. Box 10, Bellingham, WA 98225).

29. Stephani D. (1979). Monte Carlo calculations of backscattered electrons at registration marks. J. Vac. Sci. Technol. **16(6)**: 1739-1742.

30. Stephani D, Froschle E. (1978). High precision automatic alignment procedure for vector scan e-beam lithography, J. Vac. Sci. Technol. **15(3)**: 906-908.

31. Wada Y, Hisamoto Y, Mitzukami K. Migitaka M. (1981). Studies on an electron-beam mask-defect inspection system. J. Vac. Sci. Technol. **19(1)**: 36-39.

32. Wells OC. (1974). Scanning Electron Microscopy. McGraw Hill, New York.

33. Wells OC, Savoy RJ, Bailey PJ. (1982). Backscattered electron imaging in the scanning electron microscope–measurement of surface layer mass-thickness, Proceedings of the 1st Pfefferkorn Conference, Electron Beam Interaction with Solids, Op Cit., 287-298.

Discussion with Reviewers

K. Murata: You discussed various effects of electron scattering on the backscattered electron signals from a single isolated step or hole in mask inspection. Are these discussions generally applicable to the case of multiple steps or holes?
Author: Yes, as discussed in the paper I chose isolated steps and holes because they represented the limiting signals which would be observed. The scattering of electrons from multiple steps and holes would fall somewhere in between, as some electrons scattered from the sides of the structures would have other structures to pass through before scattering into the detector.

K. Murata: Have you investigated the optimum energy for mask inspection? Could you comment on the optimum energy to obtain a sharp rise-up of the signal for a specific thickness of mask material?
Author: As far as shot noise and beam stability is concerned, the highest beam energy possible would be optimum. However, one would first have to make sure that the absorber thickness was large enough to get the maximum signal at the chosen beam energy. A sharp rise-up of the signal can be achieved by collecting low angle electrons, using low beam energy, and using the smallest possible inspection beam. One would have to determine the beam current required for adequate SNR and then determine what minimum beam voltage could supply the needed current in a beam of minimum required size. Then, the detector should be placed so as to collect some of the low angle electrons. Thus, it can be seen that the optimum beam energy will be very dependent on the type of system required.

K. Murata: You assumed one detector for backscatter electron detection. Could you speculate what results you can obtain by using multiple detectors such as opposite two detectors and a quadruple type detector?
Author: I assumed an annular detector in all the calculations because the SNR of the backscattered electron signal is best when you collect as many electrons as possible. The use of two detectors would result in a loss of signal. Four detectors could be properly placed so as to collect more backscattered electrons using the same diode area as an annular detector. The main goal is to collect as many electrons as possible at the fastest speed possible (i.e., use the smallest amount of diode area possible). Keeping in mind that most detectors are energy sensitive, it can be seen that for a given number of electrons backscattered from Au and from Si, the signal from the Au will be higher since the average energy of backscattered electrons is higher from Au. Thus, the difference in signal levels between absorber and substrate increases as the number of collected backscattered electrons increases. This in turn leads to a better SNR for the signal.

K. Murata: Could you comment on the possibility of mask inspections by the absorbed electron current, comparing with those by the backscattered electrons you studied?
Author: One interesting possibility would be to look for holes in the absorber using the absorbed electron current when scanning over the absorber. The backscattered electron detector could then be used to detect excess absorber material when scanning over clear areas. The question is whether the absorbed electron current scheme would allow fast enough inspection speed (TV rate, for example). At present, I have not investigated this.

V.N.E. Robinson: The human eye is used to interpreting images with slight directionality in illumination, equivalent to a non-symmetrical detector. Your results indicate changes in intensity with collection angle. Have you any experimental results indicating ease or otherwise of interpretation of results with directional detection?
Author: I have experimental results which prove that the simulation program is correct in predicting signal variation with collection angle range. (See text ref. 26.) I have not done any work investigating the use of directional detection. As explained in an answer to K. Murata above, we really want to collect as many electrons as possible in mask inspection. However, since the signals from holes in Au are different than those from isolated Au structures, it would be interesting to use different detectors to detect different types of defects.

H. Niedrig: How did the author obtain his values for the Bethe range R_B? To my knowledge the Bethe ranges originally have not been calculated by a Monte Carlo program (which could hardly be done in the 1930s) but from a quantum mechanical treatment of the non-relativistic stopping power: H.A. Bethe (1933). Quantennemechanik der Ein- und Zwei-Elektronensysteme, in: Handbuch der Physik, Vol. 24, p. 521, H. Geiger, K. Scheel (Eds.), Springer-Verlag, Berlin, cited in: R.D. Birkhoff: The passage of fast electrons through matter, in: Handbuch der Physik, Vol. 34, p. 62, E. Flugge (Ed.), Springer-Verlag, Berlin, 1958, which is cited in author's reference 3.
Author: I obtained my values for the Bethe range by simply adding up the path lengths of an electron's trajectory in the Monte Carlo program. This yields the same results as would be obtained from the more exact method discussed above of integrating the Bethe equation.

K. Murata: Have you obtained undershoot and overshoot profiles for the signals near the edges of steps and holes, respectively, with an infinitely fine beam size?
Author: No, not yet.